Journal of Power Sources 241 (2013) 583–588

Contents lists available at SciVerse ScienceDirect

Journal of Power Sources

journal homepage: www.elsevier.com/locate/jpowsour

Electrochemical properties of an all-solid-state lithium-ion battery with an in-situ formed electrode material grown from a lithium conductive glass ceramics sheet

Yuichi Amiki [a], Fumihiro Sagane [a,b], Kazuo Yamamoto [c], Tsukasa Hirayama [c], Masao Sudoh [a], Munekazu Motoyama [b,d], Yasutoshi Iriyama [b,d,*]

[a] Department of Materials Science and Chemical Engineering, Faculty of Engineering, Shizuoka University, 3-5-1 Johoku, Naka-ku, Hamamatsu, Shizuoka 432-8561, Japan
[b] JST-ALCA, 5, Sanbancho, Chiyoda-ku, Tokyo 102-0075, Japan
[c] Nanostructures Research Laboratory, Japan Fine Ceramics Center, 2-4-1 Mutsuno, Atsuta-ku, Nagoya 456-8587, Japan
[d] Department of Materials, Physics and Energy Engineering, Graduate School of Engineering, Nagoya University, Furo-cho, Chikusa-ku, Nagoya 464-8603, Japan

HIGHLIGHTS

- Lithium insertion reaction into a lithium ion conductive solid electrolyte (LATP) sheet is investigated.
- Lithium insertion reaction into the LATP sheet occurs at 2.35 V (vs. Li/Li^+), which becomes in-situ formed electrode material.
- Charge transfer resistance at the in-situ formed electrode/LATP-sheet is less than 100 Ω cm^2.
- A multilayer of Pt/LATP-sheet/$LiCoO_2$/Au works as a battery operating at 1.5 V.
- The battery shows redox peak in the potential sweep curve even at 100 mV s^{-1} and stable charge-discharge reaction.

ARTICLE INFO

Article history:
Received 7 February 2013
Received in revised form
30 April 2013
Accepted 4 May 2013
Available online 14 May 2013

Keywords:
All-solid-state battery
Interface
Thin film
In-situ

ABSTRACT

A lithium insertion reaction in a Li^+ conductive glass ceramics solid electrolyte (lithium aluminum titanium phosphate: LATP) sheet produces an in-situ formed electrode active material, which operates at 2.35 V vs. Li/Li^+ in the vicinity of the LATP-sheet/current–collector interface. Electron energy loss spectroscopy clarifies that titanium in the LATP sheet in the vicinity of the current collector/LATP-sheet interface is preferentially reduced by this lithium insertion reaction. Charge transfer resistance between the in-situ-formed-electrode and the LATP-sheet is less than 100 Ω cm^2, which is smaller than that of the common LiPON/$LiCoO_2$ interface. A thin film of $LiCoO_2$ is deposited on one side of the LATP-sheet as a Li^+ source for developing the in-situ formed electrode material. Eventually, a Pt/LATP-sheet/$LiCoO_2$/Au multilayer is fabricated. The multilayer structure successfully works as an all-solid-state lithium-ion battery operating at 1.5 V. A redox peak of the battery is observed even at 100 mV s^{-1} in the potential sweep curve. Additionally, charge–discharge reactions are repeated stably even after 25 cycles.

© 2013 Elsevier B.V. All rights reserved.

1. Introduction

All-solid-state rechargeable lithium batteries (SSBs) using incombustible inorganic solid electrolytes are expected to be the next generation rechargeable batteries with greater safety and high energy density. However, a drawback of SSBs is their low power densities. One reason originates from the large interfacial resistances at the electrode/solid–electrolyte interfaces. Because electrodes and solid electrolytes are hard materials in general, they tend to have point contacts with each other, which inevitably reduce the number of electrochemical active sites at interfaces, thereby increasing interfacial resistance. Moreover, even if they have large contact areas, for example, using soft materials such as sulfide-based solid electrolytes, in some cases they react with each other, and a resistive mutual diffusion layer forms at the interfaces. An effective method to prevent the formation of a mutual diffusion layer is surface coating at the interface. Several coating materials have been proposed in various SSBs [1–4].

* Corresponding author. Department of Materials, Physics and Energy Engineering, Graduate School of Engineering, Nagoya University, Furo-cho, Chikusa-ku, Nagoya 464-8603, Japan.
E-mail address: iriyama@numse.nagoya-u.ac.jp (Y. Iriyama).

0378-7753/$ – see front matter © 2013 Elsevier B.V. All rights reserved.
http://dx.doi.org/10.1016/j.jpowsour.2013.05.006

An alternative approach to remedy the interface problem is to directly grow electrode active materials from a solid electrolyte. Although lithium insertion reaction into a solid electrolyte is generally recognized as a reductive-side potential window for the solid electrolyte, it can also be considered as a formation of an electrode active material from a solid electrolyte. If an electrode active material can grow from a solid electrolyte and coexist, they should have a well-connected heterogeneous interface without a resistive mutual diffusion layer, leading to the formation of a low resistive electrode/solid–electrolyte interface.

Lithium insertion reaction process into solid electrolytes depends on the species of solid electrolytes. For example, perovskite-structured lanthanum lithium titanate (LLT) is well-known high Li^+ conductive solid electrolyte [5], but fast coloration of the entile LLT pellet occurs when a partial lithium insertion reaction into the LLT pellet is carried out [6]. Hence, it is difficult to create the coexistence of a parent solid electrolyte with a lithium inserted region. On the other hand, in the case of a Li^+ conductive glass ceramics solid electrolyte sheet based on NASICON-type structure $LiTi_2(PO_4)_3$ (LATP sheet; manufactured by OHARA Inc. Kanagawa, Japan) [7], lithium insertion reactions preferentially take place around solid-electrolyte/current–collector interface. Because the lithium inserted-regions (electrode active material) do not spread easily inside the parent LATP sheet (solid electrolyte) [8,9], this approach is regarded as more feasible compared to a method using LLT.

In previous work, we have focused on this latter case to date and have reported that an SSB using a partially lithium inserted LATP sheet as an electrode active material works as a battery [8,9]. However, because this electrode active material initially required a large irreversible capacity to be developed, our past works focused on the battery manufacturing process to prevent and/or apply this irreversible capacity. The aim of this work is to investigate the lithium insertion/extraction reaction into the LATP sheets. We especially focus on charge transfer reaction. We show that the in-situ-formed electrode/LATP-sheet interfacial resistance is reduced to less than 100 Ω cm^2, which is smaller than that of the common $LiCoO_2$/LiPON interface (~ 150 Ω cm^2) [10]. Moreover, lower electronic conductivity of the in-situ-formed electrode active material tends to prevent the excessive growth of electrode material toward the LATP sheet, which restrains the irreversible capacity loss after the second cycle. Additionally, electrochemical properties of the Pt/LATP-sheet/$LiCoO_2$/Au multilayer are investigated.

2. Experimental

Mirror-polished LATP sheets [7] (150 μm in thickness) were used as solid electrolytes in this study. The Li^+ conductivity of the LATP sheet is 1×10^{-4} S cm^{-1} at room temperature. The crystalline phase presented in the LATP sheet is a mixture of $Li_{1+x}Al_xGe_yTi_{2-x-y}P_2O_{12}$ (main-phase), $Li_{1+x+3z}Al_x(Ge,Ti)_{2-x}(Si_zPO_4)_3$ (sub-phase), and $AlPO_4$. The former two phases have been indexed using $LiTi_2(PO_4)_3$ with a NASICON-type structure in XRD. Details on this sheet have been precisely reported in other papers [11,12]. Thin films of $LiCoO_2$ were deposited on one side of the LATP sheet by pulsed laser deposition at 873 K for 1, 3, 5, and 8 h (the deposition rate is ~0.1 μm per hour). Then, thin films of platinum (Pt) or gold (Au) were covered on these film electrodes as current collectors by RF magnetron sputtering. The opposite side of the LATP sheet was covered with a Pt thin film. As will be described below, partial Li^+ insertion reaction into the LATP sheet near the Pt/LATP-sheet interface produces the in-situ-formed Li^+ insertion electrode active material. Thus, any electrode active material is not presented at Pt/LATP-sheet interface in pristine state.

Electrochemical properties of the two kinds of half-cells, that is, Pt/LATP-sheet and LATP-sheet/$LiCoO_2$/Pt, were measured by cyclic voltammetry (CV), charge-discharge reaction, and AC impedance spectroscopy at room temperature using a three-electrode cell. The bare side of the LATP sheet in each half cell was immersed in propylene carbonate containing 1 mol dm^{-3} $LiClO_4$ (EL-PC), while the opposite Pt or $LiCoO_2$ side was mounted on a stainless steel substrate. Reference and counter electrodes were lithium (Li) immersed in the EL-PC. The electrochemical apparatus used in these experiments is schematically shown in Fig. 1. The LATP sheet is a liquid-tight sheet, and this cell configuration includes an interfacial Li^+ transfer reaction at the EL-PC/LATP-sheet interface. This interfacial resistance was investigated using a Li/EL-PC/LATP-sheet/EL-PC/Li symmetrical non-blocking electrode cell [13]. Hereafter, electrode potential of electrochemical properties using half cells will be referred to as the Li/Li^+. The electrochemical properties of a multilayer of Pt/LATP-sheet/$LiCoO_2$/Au (SSLIB) were measured in the same manner, but, in this case, the voltage of the SSLIB was measured. The electrode area of the Li/EL-PC/LATP-sheet/EL-PC/Li cell is 0.4 cm^2, and that of other cells is 0.785 cm^2.

Electron energy loss spectroscopy (EELS) analysis with a 200 kV transmission electron microscope (TEM, JEM-2100F) was performed to evaluate the electronic state of a transition metal element Ti included in the cycled LATP sheet. The Pt/LATP side of the SSLIB was partially thinned with a focused ion beam system (FIB, FB-2100), and the potential sweep measurement (sweep rate: 0.67 mV s^{-1}) of the TEM sample was carried out in the TEM [14]. After the initial cycle, the TEM sample was maintained by a short circuit, and then the EELS spectra of Ti $L_{2,3}$-edge were obtained from the two points; one is approximately 1.5 μm apart from the Pt/LATP interface and the other is near the interface where the lower electric-potential was previously observed by electron holography [15].

3. Results and discussions

3.1. Electrochemical properties of the Pt/LATP-sheet half cell

Fig. 2(a) shows the CV of the lithium insertion/extraction reactions of the Pt/LATP-sheet half-cell:, a couple of redox peaks were observed at 2.35 V. This indicates that part of the LATP sheet works as an electrode active material [8,9]. This redox potential is nearly the same with $LiTi_2(PO_4)_3$ (LTP) where lithium insertion/extraction reactions take place at 2.5 V (vs. Li/Li^+) via a two-phase reaction between LTP and $Li_3Ti_2(PO_4)_3$ [16,17]. Fig. 2(b) shows initial lithium insertion/extraction curves of the LATP sheet. A potential plateau was observed near 2.35 V, and large irreversible capacity was observed. This indicates that the lithium-inserted region does not recover to the original solid electrolyte, thus, the LATP sheet is

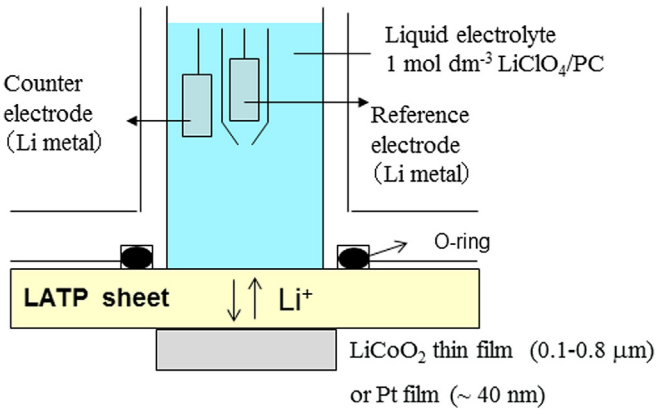

Fig. 1. Schematic image of an electrochemical measurement system for half-cells.

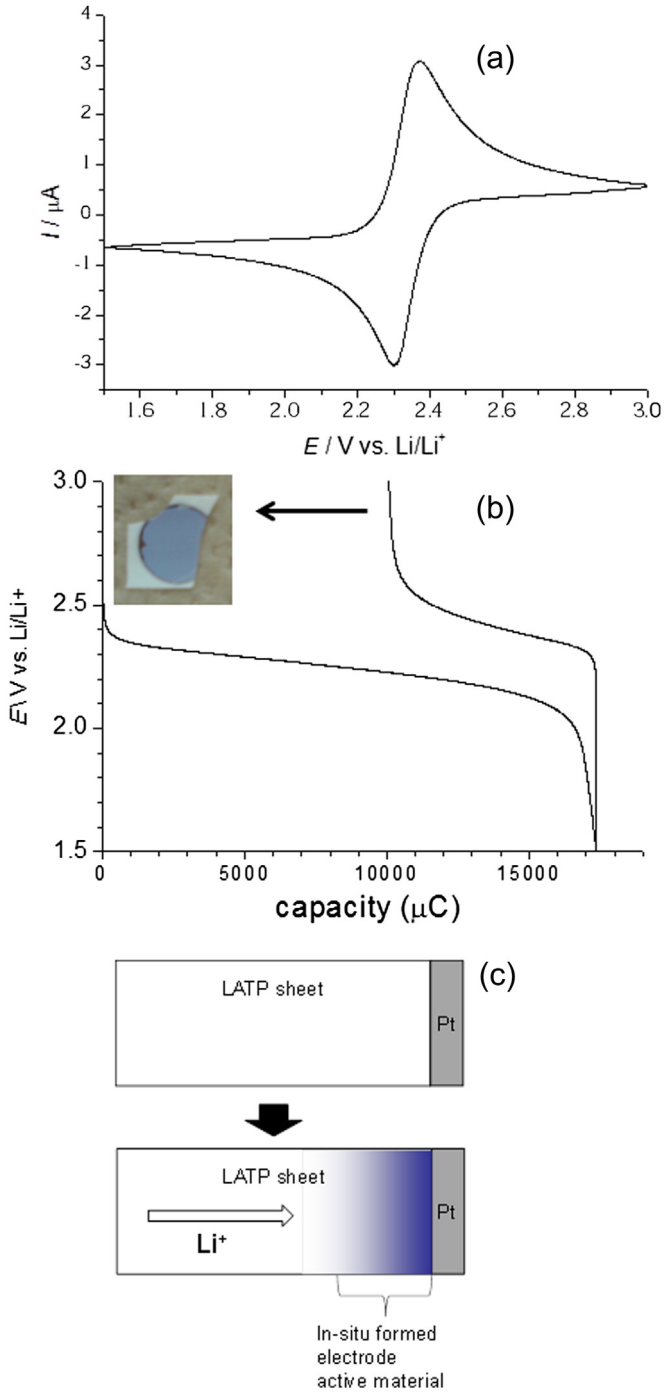

Fig. 2. (a) Initial CV of the Pt/LATP-sheet half cell at 3.0–1.5 V. $v = 0.1$ mV s^{-1}. (b) Initial lithium insertion/extraction curve of Pt/LATP-sheet half cell. $I = 1$ μA. $A = 0.785$ cm^2. (c) Schematic image of lithium insertion reaction to the Pt/LATP-sheet half cell.

partially decomposed. The inset in Fig. 2(b) shows an optical microscope image of the LATP sheet after this charge-discharge cycle, where the Pt thin film was removed with adhesive tape in an argon-filled glove box. The lithium-inserted region changed its original white color to blue, while the original color was maintained on the opposite side (EL-PC side).

Fig. 2(c) shows the lithium insertion reaction into the LATP sheet schematically. As will be described in later, in-situ-formed electrode material itself seems to have low electronic conductivity. Moreover, in case of the LTP, electronic conductivity is reduced at the charging (oxidation) process. When the reducing of the electronic conductivity takes place for the in-situ-formed electrode material, the electrochemical charging reaction will be reduced by further reduction of the electronic conductivity and the retardation of its charging reaction. This may be another reason for low coulomb efficiency, especially in the initial cycle.

Fig. 3(a) shows a cross-sectional TEM image of the Pt/LATP-sheet interface after the formation of an in-situ formed electrode material by the potential sweep method with the SSLIB between 0.0 and 2.0 V ($v = 0.67$ mV s^{-1}). Measurements of Ti $L_{2,3}$-edge EELS analysis were carried out at both A and B. The spectrum measured at A (approximately 1.5 μm away from the interface) was in good agreement with the pristine LATP sheet, in which shoulder peaks typically observed for Ti^{4+} were recognized [18]. On the other hand, the spectrum at B (beside the Pt/LATP-sheet interface) was shifted to lower energy-loss direction, indicating that Ti^{4+} was reduced in this area. This reduction indicates that the lithium insertion reaction preferentially occurred in the vicinity of the Pt/LATP-sheet interface. Our previous electron holography experiments suggested that the thickness of the in-situ-formed electrode material grown from the interface was 0.7 μm [15]. Thus, this EELS analysis reasonably agrees with the past result. When the in-situ-formed

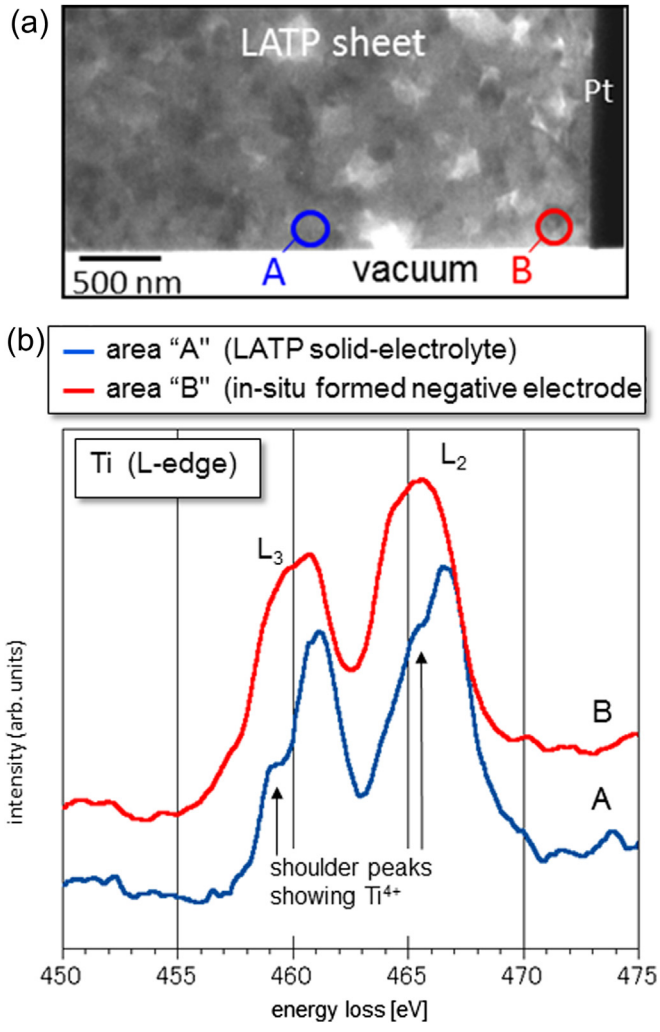

Fig. 3. (a)Cross-sectional TEM image around the Pt/LATP-sheet after the Li^+ insertion reaction by the potential sweep method using a Pt/LATP-sheet/$LiCoO_2$/Au battery. $v = 0.67$ mV sec^{-1}. (b) Ti $L_{2,3}$-edge EELS spectra measured at the circles A and B in Fig. 3(a).

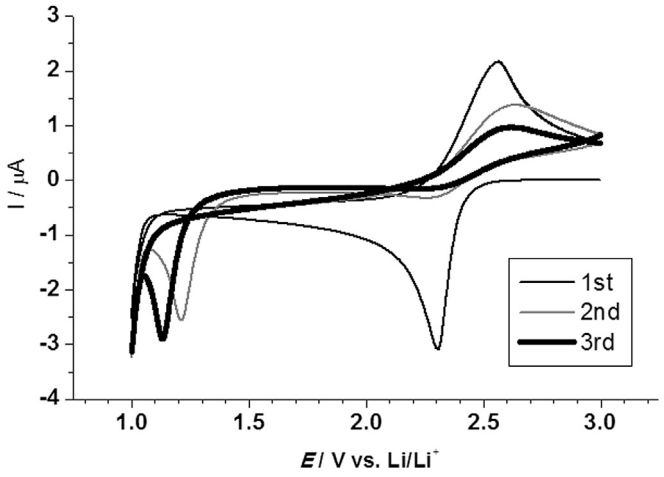

Fig. 4. CVs of the Pt/LATP-sheet half cell at 3.0–1.0 V measured sequentially for three cycles. $A = 0.785\ cm^2$ $v = 0.1\ mV\ s^{-1}$.

electrode material grows in this region (0.7 μm), the lithium inserted capacity at the 1st cycle is estimated to be 67 mAh g^{-1}.

Fig. 4 shows the CVs measured continuously between 3.0 V and 1.0 V. A reductive current peak at 2.3 V was observed as with Fig. 2(a) in the initial Li^+ insertion process, but in later cycles, this peak almost disappeared, and an alternative peak appeared at around 1.2 V. This means that a further lithium insertion reaction does not occur around the front edge of the in-situ formed electrode material in the LATP sheet; rather, the reaction will still preferentially take place around the in-situ-formed-electrode/Pt interface. This is probably because electronic conductivity in the in-situ formed electrode material is smaller than the lithium ionic conductivity in it. Our past electron holography experiments show that the potential drops with the approach to the Pt/LATP-sheet interface at 2.0 V in the SSLIB, at which further lithium insertion reaction is carried out to the in-situ formed electrode material below 2.3 V [15]. This result also supports the above-mentioned lithium insertion process. This insertion process in turn increases the lithium concentration in the in-situ-formed electrode at the interface, which will lead to the potential drop to 1.2 V shown in Fig. 4. This situation may resemble the lithium insertion reaction into $Li_3Ti_2(PO_4)_3$, the end member of the two-phase reaction with LTP, which occurs at 1.0 V (vs. Li/Li^+). Low electronic conductivity but with high ionic conductivity of the in-situ formed electrode material will retard its growth toward the LATP sheet and then coexist with the parent LATP sheet working as a solid electrolyte.

Fig. 5(a) shows AC impedance spectra of the Pt/LATP-sheet half-cell at different potentials. This half-cell contains various resistive and capacitive elements in electrolytes (liquid electrolyte and LATP sheet) and interfaces (EL-PC/LATP-sheet and LATP-sheet/in-situ-formed-electrode). However, only the LATP-sheet/in-situ-formed-electrode interface should have a potential dependence. Thus, the semicircular arc newly appearing in the lowest frequency range is assigned to charge transfer resistance at this interface. The estimated interfacial resistivity at 2.34 V is less than 100 Ω cm^2, which is smaller than that of the previously reported LiPON/$LiCoO_2$ interface (150 Ω cm^2) [10]. This result indicates that in-situ formation of an electrode material from a solid electrolyte interface is an effective method to develop a low-resistive interface. The semicircular arc at a high frequency range is composed of the resistances of electrolytes. The interfacial Li^+ transfer resistance at the LATP-sheet/EL-PC interface was estimated using a Li/EL-PC/LATP-sheet/EL-PC/Li symmetrical cell. The AC impedance

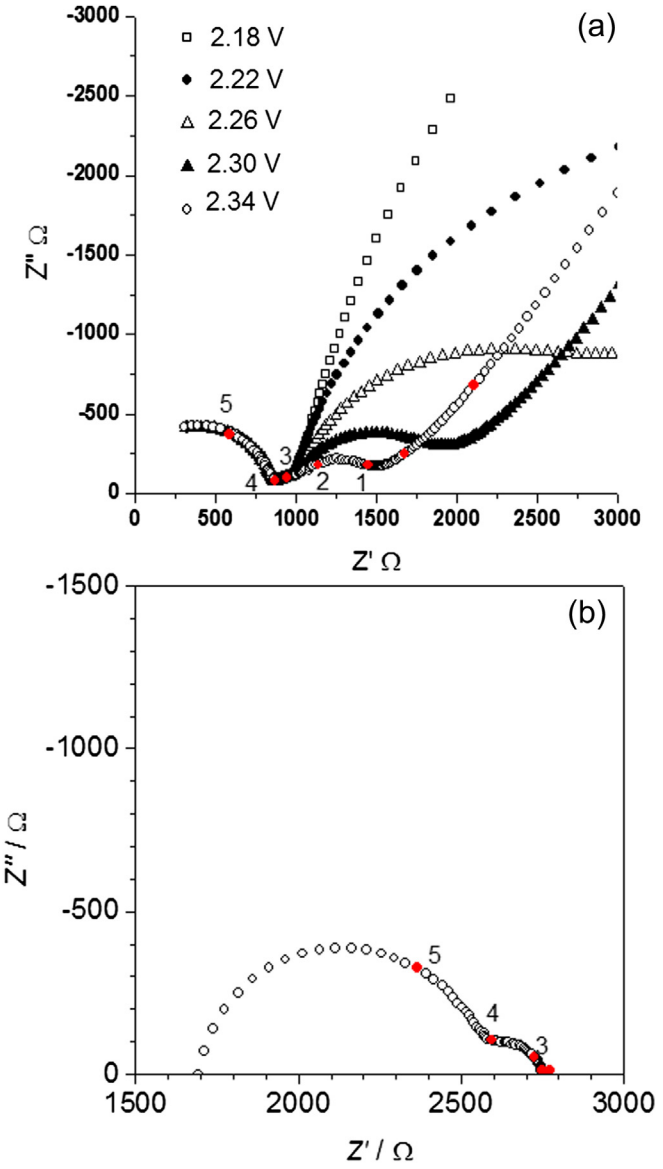

Fig. 5. AC impedance spectra of the (a) Pt/LATP-sheet half cell at 2.18 V (□), 2.22 V (■), 2.26 V (△), 2.30 V (▲), and 2.34 V (○) (vs. Li/Li^+) and (b)Li/EL-PC/LATP-sheet/EL-PC/Li symmetrical cell at 0 V. $A = 0.4\ cm^2$ in both sides. Closed data pointes in Fig. 5(a) at 2.34 V and in Fig. 5(b) at 0 V were measured at 10^n Hz. (b).

spectrum of this symmetrical cell is shown in Fig. 5(b), where the semicircular arc observed at the lowest frequency is assigned to the EL-PC/LATP-sheet interfacial resistance [13]. Hence, this component will be attributed to the semicircular arc with a characteristic frequency in an intermediate frequency on the order of 10^3 Hz in Fig. 5(a).

3.2. Charge–discharge properties of the Pt/LATP-sheet/$LiCoO_2$/Au

As described in the previous subsection, the in-situ formed electrode material shows redox potential at 2.35 V (vs. Li^+/Li), while that of the $LiCoO_2$ is at 4 V [19]. Therefore, when these two electrode active materials are combined in an all-solid-state lithium-ion battery (SSLIB: Pt/LATP-sheet/$LiCoO_2$/Au), the in-situ formed electrode material will work as negative electrode material, with $LiCoO_2$ as a positive electrode. Fig. 6 summarizes the charging curves of $LiCoO_2$ thin film with 0.1, 0.3, and 0.5 μm in thickness

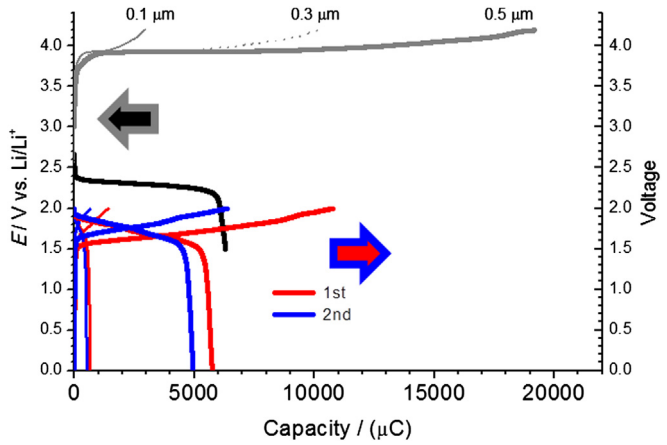

Fig. 6. Lithium extraction curve of LATP-sheet/$LiCoO_2$ (0.1 μm (thin gray line), 0.3 μm (dotted gray line), and 0.5 μm (bold gray line) in thickness) half cell at first cycle and lithium insertion curve of Pt/LATP-sheet half cell at second cycle (bold black line). $I = 1$ μA. $A = 0.785$ cm^2. Red (1st cycle) and blue (2nd cycle) lines show charge-discharge curves of the Pt/LATP-sheet/$LiCoO_2$/Au battery using 0.1 μm- (thin lines) and 0.5 μm-(bold lines) $LiCoO_2$ thin films between 2.0 V and 0 V. $I = 1$ μA. $A = 0.785$ cm^2. (For interpretation of the references to color in this figure legend, the reader is referred to the web version of this article.)

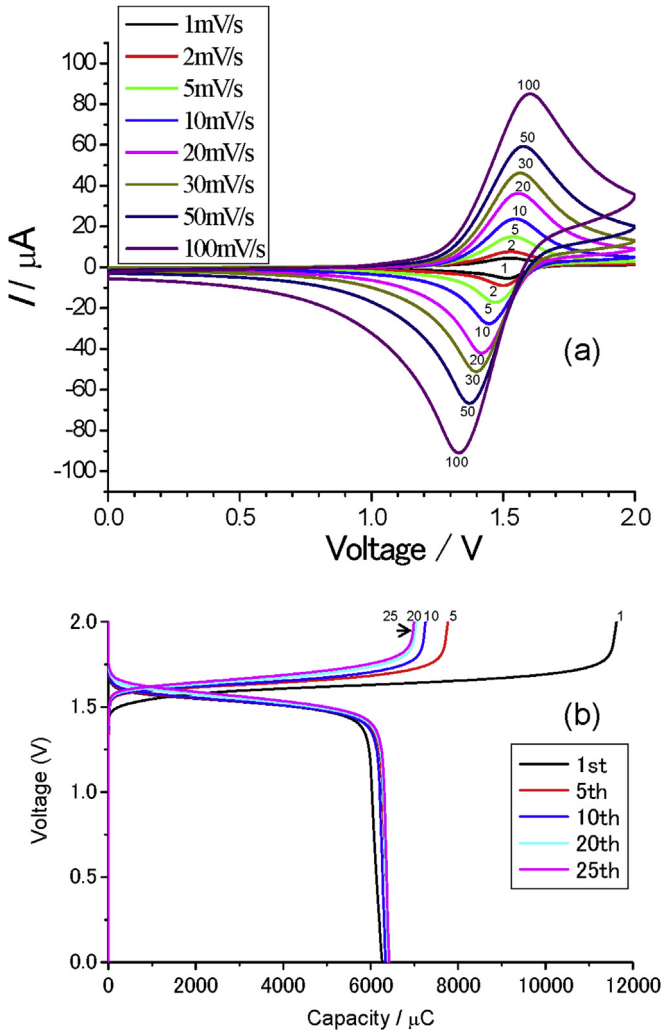

Fig. 7. (a) Potential sweep curves of an all-solid state lithium ion battery (Pt/LATP-sheet/$LiCoO_2$ (0.8 μm in thickness)/Au at different sweep rates. (b) Charge–discharge curves of the battery. $I = 1$ μA. $A = 0.785$ cm^2.

(gray lines), second discharging curve of the in-situ formed electrode material (black line), and charge-discharge curves of SSLIBs with 0.1 μm- or 0.5 μm-thick $LiCoO_2$ thin-film electrodes at the 1st and 2nd cycles (red and blue lines, respectively), where current was 1 μA in all cases. In both SSLIBs, charge–discharge reactions take place at around 1.7 V, which is a reasonable value when considering the difference of the redox potential of $LiCoO_2$ and the in-situ-formed electrode material. The initial discharge capacity of the SSLIB with 0.5 μm-thick $LiCoO_2$ is a comparable value to the second discharge capacity of the in-situ-formed negative electrode material because sufficient amount of Li^+ is stored in the $LiCoO_2$ film. Then, the capacity of this battery is limited by the growth amount of the in-situ formed electrode material. On the other hand, the discharge capacity of the SSLIB with 0.1 μm-thick $LiCoO_2$ is much smaller because the capacity of the 0.1 μm-thick $LiCoO_2$ is smaller than the possible growth amount of the in-situ-formed electrode material. This capacity is then limited by the Li^+-supplying quantity of $LiCoO_2$. In both SSLIBs, the irreversible capacity of approximately half the initial charging capacity is due to the development of the in-situ-formed electrode material, as mentioned in the previous subsection. This irreversible capacity means the consumption of Li^+ in $LiCoO_2$, and then the lithium composition, x in Li_xCoO_2, becomes less than 1 after the initial discharge reaction. Thus, at the second charging process, the Li^+ extraction reaction starts from Li_xCoO_2 ($x < 1$) at higher voltage than with $x = 1$. Therefore, charging voltage during the second cycle achieves a higher value than that of the first cycle. As can be expected from these results, the charge-discharge capacity and the voltage of the SSLIB is influenced by the thickness of $LiCoO_2$.

Fig. 7(a) shows the potential sweep curves of the SSLIB with 0.8 μm-thick $LiCoO_2$ film. The redox peak due to charge-discharge reaction is observed at 1.5 V. Because this redox capacity is governed by the in-situ-formed electrode material with relatively small interfacial resistivity, redox peak is observed clearly even at 100 mV s^{-1}. Fig. 7(b) shows the cycle performances of this SSLIB, and stable charge-discharge reactions were repeated for at least 25 cycles.

4. Conclusion

A lithium insertion reaction into a Li^+ conductive solid electrolyte sheet, a LATP sheet, was carried out, and electrode active material was grown in-situ from the LATP sheet. The resultant electrode material was developed around the LATP-sheet/Pt (current collector film) interface with a thickness of less than 1.5 μm from the interface and was operated at 2.35 V vs. Li/Li^+. Interfacial resistivity at the in-situ-formed-electrode/LATP-sheet interface was less than 100 Ω cm^2 at 2.34 V vs. Li/Li^+, which was smaller than that of the $LiCoO_2$/LiPON interface. This indicates that the in-situ formation of electrode active material from solid electrolyte is an effective method to produce a low-resistive interface between an electrode and a solid electrolyte interface. This small interfacial resistivity is attributed to a well-connected electrode/solid–electrolyte interface due to the in-situ growth of electrode material from solid electrolyte. Multiple layers of Pt/LATP-sheet/$LiCoO_2$ (0.8 μm in thickness)/Au became an all-solid-state lithium-ion battery operating at 1.5 V and repeated stable lithium insertion–extraction reactions for at least 25 cycles.

Acknowledgments

This work was financially supported by JST-ALCA and in-part by NEDO-RISING. The authors would like to give special thanks to Dr. Toru Asaka, Nagoya Institute of Technology, for his help with EELS measurements.

References

[1] N. Ohta, K. Takada, L.Q. Zhang, R.Z. Ma, M. Osada, T. Sasaki, Adv. Mater. 18 (2006) 2226.
[2] N. Ohta, K. Takada, I. Sakaguchi, L.Q. Zhang, R.Z. Ma, K. Fukuda, M. Osada, T. Sasaki, Electrochem. Commun. 9 (2007) 1486.
[3] A. Sakuda, A. Hayashi, M. Tatsumisago, Chem. Mater. 22 (2010) 949.
[4] T. Kato, T. Hamanaka, F. Sagane, K. Yamamoto, T. Hirayama, M. Motoyama, and Y. Iriyama, submitted for publication.
[5] Y. Inaguma, L.Q. Chen, M. Itoh, T. Nakamura, T. Uchida, H. Ikuta, M. Wakihara, Solid State Commun. 86 (1993) 689.
[6] P. Birke, S. Scharner, R.A. Huggins, W. Weppner, J. Electrochem. Soc. 144 (1997) L167.
[7] http://www.ohara-inc.co.jp/jp/product/electronics/licgc.html.
[8] Y. Iriyama, C. Yada, T. Abe, Z. Ogumi, K. Kikuchi, Electrochem. Commun. 8 (2006) 1287.
[9] C. Yada, Y. Iriyama, T. Abe, K. Kikuchi, Z. Ogumi, Electrochem. Commun. 11 (2009) 413.
[10] Y. Iriyama, T. Kako, C. Yada, T. Abe, Z. Ogumi, J. Power Sources 146 (2005) 745.
[11] J. Fu, J. Am. Ceram. Soc. 80 (1997) 1901.
[12] https://www.ornl.gov/ccsd_registrations/battery/presentations/Session8-240-Nakajima.pdf.
[13] T. Abe, F. Sagane, M. Ohtsuka, Y. Iriyama, Z. Ogumi, J. Electrochem. Soc. 152 (2005) A2151.
[14] K. Yamamoto, Y. Iriyama, T. Asaka, T. Hirayama, H. Fujita, C.A.J. Fisher, K. Nonaka, Y. Sugita, Z. Ogumi, Angew. Chem. Int. Ed. 49 (2010) 4414.
[15] K. Yamamoto, Y. Iriyama, T. Asaka, T. Hirayama, H. Fujita, K. Nonaka, K. Miyahara, Y. Sugita, Z. Ogumi, Electrochem. Commun. 20 (2012) 113.
[16] C. Delmas, A. Nadiri, Mater. Res. Bull. 23 (1988) 65.
[17] S. Patoux, C. Masquelier, Chem. Mater. 14 (2002) 5057.
[18] A. Ohtomo, D.A. Muller, J.L. Grazul, H.Y. Hwang, Nature 419 (2002) 378.
[19] K. Mizushima, P.C. Jones, P.J. Wiseman, J.B. Goodenough, Mat. Res. Bull. 15 (1980) 783–789.